Journal of Power Sources 190 (2009) 453–460

Contents lists available at ScienceDirect

Journal of Power Sources

journal homepage: www.elsevier.com/locate/jpowsour

Evolution of stress within a spherical insertion electrode particle under potentiostatic and galvanostatic operation

Yang-Tse Cheng[a,*], Mark W. Verbrugge[b]

[a] Department of Chemical and Materials Engineering, University of Kentucky, Lexington, KY 40506, USA
[b] Materials and Processes Lab., General Motors Research and Development Center, Warren, MI 48090, USA

ARTICLE INFO

Article history:
Received 18 November 2008
Received in revised form 10 January 2009
Accepted 12 January 2009
Available online 21 January 2009

Keywords:
Stress
Strain energy
Diffusion
Galvanostatic
Potentiostatic
Battery

ABSTRACT

Lithium ion battery electrode materials generally experience significant volume changes during charging and discharging caused by concentration changes within the host particles. Electrode failure, in the form of fracture or decrepitation, may occur as a result of a highly localized stress, strain energy, and stress cycles over time. In this paper, we develop analytic expressions for the evolution of stress and strain energy within a spherically shaped electrode element under either galvanostatic (constant current) or potentiostatic (constant potential) operation when irreversible phenomena are dominated by solute diffusion resistance within host particles. We show that stresses and strain energy can evolve quite differently under potentiostatic vs. galvanostatic control. The findings of this work suggest the possibility of developing new battery charging strategies that minimize stress and strain energy and thus prolong battery life.

1. Introduction

Diffusion-induced stress (DIS) can occur as a result of compositional inhomogeneities during solid-state diffusion in many technological situations, including dopant diffusion in semiconductor processing, oxidation of metals, hydrogen transport in solid-state hydrogen-storage media, and lithium diffusion in battery electrodes. Several authors have developed models for DIS. For example, Prussin [1] made an analogy between thermal stress and DIS and analyzed the transverse stresses developed in a thin plate during mass transfer. Li [2] provided a number of analytical solutions to DIS problems in spherical, cylindrical, and thin plate geometry. Lee and co-workers [3–5] have also studied DIS in various systems including thin plates, hollow cylinders, and composites. Yang and Li [6,7] considered the effect of diffusion-induced stresses on the bending of beam and plate structures for sensing applications. Yang also studied the coupled problem of interactions of stress and diffusion [7].

Within the electrochemical energy storage topical area, a number of publications address the modeling of lithium ion batteries [8–15] and are focused on the underlying thermodynamics, interfacial kinetics, and transport phenomena governing electrochemical systems in the context of a volume-averaged treatment of porous media. Recently, García et al. [16], Christensen and Newman [17,18] and Zhang et al. [19] studied stresses generated during Li diffusion under galvanostatic control. The latter authors also investigated linear sweep voltammetry of a single particle as well as heat generation [20]; their investigation included spherical and ellipsoidal particles. The paper by Zhang et al. [21] is devoted to the analysis of a single particle undergoing electrochemical insertion and outlines the motivation for such single particle studies. The aforementioned battery references and this work are motivated by the need to develop high energy and power batteries that are durable over the intended usage profiles [24].

Since batteries are usually charged using sophisticated methods that consist of both galvanostatic and potentiostatic control, we report in this paper stress and strain energy evolution under either purely galvanostatic or potentiostatic condition when the resistance of the cell is governed by solute diffusion limitations within the insertion particles. The analytic solutions developed in this work should improve the current understanding of stress and strain energy evaluation by (1) identifying dimensionless parameters that control stress and strain energy evolution, (2) providing the asymptotic behavior for short- and long-time limits, and (3) rendering order of magnitude estimates for more complicated operating conditions. The results of this work may be used to develop strategies that minimize stress-induced battery failures. Additional information on relevant past works by the present authors can be found in Refs. [22,23]; in these two investigations, surface tension

* Corresponding author.
E-mail addresses: ycheng@engr.uky.edu (Y.-T. Cheng), mark.w.verbrugge@gm.com (M.W. Verbrugge).

0378-7753/$ – see front matter © 2009 Elsevier B.V. All rights reserved.
doi:10.1016/j.jpowsour.2009.01.021

Nomenclature

List of symbols

a_s	specific surface (e.g., $cm^2\ cm^{-3}$)
C	molar concentration
C_0	initial (uniform) solute concentration
C_R	surface concentration during constant potential operation
$C_{av}(r)$	average concentration in the spherical volume of radius r
$C_{av}(R)$	average concentration in the spherical particle of radius R
D	diffusion coefficient of the solute
E	Young's modulus
E_T	total elastic energy stored in the sphere of radius R
e	strain energy density
e^-	electron
F	Faraday's constant
H^+	proton
I	current over a spherical particle of radius R
I_{cell}	cell current
$i_{0,ref}$	exchange current based on reference concentration
L	electrode thickness
Li^+	lithium ion
r, θ, ϕ	spherical coordinates
R	radius of spherical particle
S	vacant site in host materials
u	radial displacement
x	dimensionless radial position

Greek symbols

ε_r	radial strain
ε_θ	tangential strain
θ_1	volume fraction of active material in porous electrode
σ_r	radial stress
σ_θ	tangential stress
σ	mean stress
$\sigma_{r,\max}$	maximum radial stress
$\sigma_{\theta,\max}$	maximum tangential stress
$\sigma_{shear,\max}$	maximum shear stress
ν	Poisson's ratio
Ω	partial molar volume of the solute
ζ_r^V	dimensionless stress in the radial direction for potentiostatic operation
ζ_θ^V	dimensionless stress in the tangential direction for potentiostatic operation
ζ_r^I	dimensionless stress in the radial direction for galvanostatic operation
ζ_θ^I	dimensionless stress in the tangential direction for galvanostatic operation
τ	dimensionless time
$\prod^V$	dimensionless total elastic energy in the sphere for potentiostatic operation
$\prod^I$	dimensionless total elastic energy in the sphere for galvanostatic operation

and surface modulus were shown to play a significant role in the determination of the stress amplitude and distribution for small particles. For the purposes of this work, we shall not include the surface phenomena, allowing us to streamline the exposition and focus on the distinguishing differences between potentiostatic and galvanostatic operation.

2. Analysis and results

2.1. Mechanics of composition induced stresses

We consider stress caused by diffusion within a spherical particle of radius R. The bulk of the spherical particle is assumed to be an isotropic linear elastic solid. Using the analogy between thermal and DIS [1–7,17–20,22,23,25], the stress–stain relationships, expressed in the spherical coordinate system, for the radial and tangential components, are

$$\varepsilon_r = \frac{1}{E}(\sigma_r - 2\nu\sigma_\theta) + \frac{1}{3}\Omega C, \qquad \varepsilon_\theta = \frac{1}{E}[(1-\nu)\sigma_\theta - \nu\sigma_r] + \frac{1}{3}\Omega C, \tag{1}$$

where E is Young's modulus, ν is Poisson's ratio, C is molar concentration, and Ω is the partial molar volume of the solute. We further assume that the elastic properties are independent of the concentration C.

Because of spherical symmetry, the radial and tangential strains, in the infinitesimal formulation of deformation, are given by $\varepsilon_r = du/dr$ and $\varepsilon_\theta = u/r$, where u is the radial displacement. Since atomic diffusion in solids is a much slower process than elastic deformation, mechanical equilibrium is established much faster than that of diffusion. Mechanical equilibrium is, therefore, treated as a static equilibrium problem. In the absence of any body-force, the equation for static mechanical equilibrium in the bulk of a sphere is given by Ref. [25]:

$$\frac{d\sigma_r}{dr} + 2\frac{\sigma_r - \sigma_\theta}{r} = 0. \tag{2}$$

The solutions for the normal and tangential stresses that satisfy the boundary condition $\sigma_r(R) = 0$ and remain finite at $r = 0$ are given by:

$$\sigma_r(r) = \frac{2E\Omega}{9(1-\nu)}[C_{av}(R) - C_{av}(r)],$$

$$\sigma_\theta(r) = \frac{E\Omega}{9(1-\nu)}[2C_{av}(R) + C_{av}(r) - 3C(r)], \tag{3}$$

where $C_{av}(r) \equiv (3/r^3)\int_0^r r^2 C(r)\,dr$ is the average concentration in the spherical volume of radius r within the particle of radius R. Since $\lim_{r\to 0} C_{av}(r) = C(0)$, Eq. (3) shows that the stress-state at the center of the sphere is purely hydrostatic, i.e., $\lim_{r\to 0}\sigma_r(r) = \lim_{r\to 0}\sigma_\theta(r)$, which is true for any physically admissible concentration profile.

Recognizing that $\sigma_\theta(r) = \sigma_\phi(r)$, we can write the "mean" stress as

$$\sigma(r) = \frac{\sigma_r(r) + 2\sigma_\theta(r)}{3} = \frac{2E\Omega}{9(1-\nu)}[C_{av}(R) - C(r)]. \tag{4}$$

Because of the spherical symmetry, one principal shear stress is zero and the other two are both equal to $(\sigma_r - \sigma_\theta)/2$. Eq. (3) shows that the principal shear stress is

$$\frac{\sigma_r(r) - \sigma_\theta(r)}{2} = \frac{E\Omega}{6(1-\nu)}[C(r) - C_{av}(r)]. \tag{5}$$

Hence, the stresses at any given location and time can be obtained once composition profile is known.

From the stresses, we can calculate the strain energy per unit volume or strain energy density $e(r)$ accumulated as a result of the elastic deformation for the isotropically deformed sphere [25]:

$$e(r) = \frac{\sigma_r^2(r) + 2\sigma_\theta^2(r) - 2\nu\sigma_\theta(r)[2\sigma_r(r) + \sigma_\theta(r)]}{2E}. \tag{6}$$

The total elastic energy stored in the sphere, E_T, which provides the driving force for fracture, can then be obtained by integrating the strain energy density over the entire volume of the spherical

particle:

$$E_T = 4\pi \int_0^R e(r) r^2 \, dr. \tag{7}$$

2.2. Diffusion-induced stresses under constant voltage and current conditions

We consider reactions of the type

$$Li^+ + e^- + S = [Li\text{–}S] \quad \text{and} \quad H^+ + e^- + S = [H\text{–}S],$$

reflecting the insertion and extraction of lithium ions (as in lithium ion cells) or protons (as in nickel metal hydride cells), respectively, two cases of immediate interest for battery systems. A vacant site with the host materials is represented by S and e^- refers to the electron. The number of electrons taking place in the electrochemical reaction and the stoichiometric coefficient of the reacting species are taken to be unity, consistent with the stated elementary reactions. When the current is controlled and the electrode resistance is governed by diffusion limitations within the insertion particles, the cell current I_{cell} is related to the current over a spherical particle by $I = I_{cell}/(a_s L)$, where the specific surface a_s (commonly expressed in units of $cm^2\ cm^{-3}$) is given by $3\theta_1/R$ [26], with θ_1 representing the volume fraction of the active material in the porous electrode and L being the porous electrode thickness. We shall assume the current density is uniform over the particle surface and we shall not account for changes in surface area of the particle during insertion and extraction in terms of impacting the current density [18], consistent with the infinitesimal formulation of deformation. When the electrode voltage is controlled relative to a reference electrode and, again, particle resistance dominates, the electrode voltage sets the solute surface concentration if the magnitude of the dimensionless group $i_{0,ref}R/[FD(C_R - C_0)]$ is large, as this group characterizes solute diffusion resistance within the host particle to that of the electrochemical reaction resistance over the particle surface [26]. In this relation, C_0 is the initial (uniform) solute concentration, C_R is the surface concentration during the constant potential operation, D refers to the diffusion coefficient of the solute, and F is Faraday's constant. The exchange current, which houses the interfacial rate constants, is rendered as $i_{0,ref}$, where the subscript "ref" indicates that it is based on reference concentrations. General texts can be consulted for a description of the interfacial charge-transfer theory [27,28]. To summarize, when solute-diffusion control prevails and the electrode is subjected to galvanostatic (controlled current) operation, the current density over the particle surface $I = FD(dC/dr)$ is fixed. Similarly, when solute-diffusion control prevails and the electrode is subjected to potentiostatic (controlled potential) operation and the dimensionless group $i_{0,ref}R/[FD(C_R - C_0)]$ is large (e.g., for facile interfacial reactions, electrodes constructed with large particles, a low solid-phase lithium diffusion coefficient, or for any combinations of these situations), the surface concentration is a constant and can be determined from an equilibrium potential relation. A specific treatment of equilibrium relations based on molecular thermodynamics for intercalation electrodes can be found in Refs. [29–31].

To illustrate the differences in stress evolution under galvanostatic and potentiostatic control, we consider a simple problem of diffusion within a sphere of radius R with a constant diffusion coefficient. The relevant diffusion equation in the spherical coordinate system is given by Ref. [32]:

$$\frac{\partial C}{\partial t} = \frac{D}{r^2}\frac{\partial}{\partial r}\left(r^2 \frac{\partial C}{\partial r}\right), \tag{8}$$

The initial and boundary conditions corresponding to potentiostatic control are given by:

$$\begin{aligned} &C(r,0) = C_0, \quad \text{for } 0 \le r \le R \\ &C(R,t) = C_R, \quad \text{for } t \ge 0 \\ &C(0,t) = \text{finite}, \quad \text{for } t \ge 0 \end{aligned}. \tag{9}$$

The initial and boundary conditions corresponding to galvanostatic control are given by:

$$\begin{aligned} &C(r,0) = C_0, \quad \text{for } 0 \le r \le R \\ &D\frac{\partial C(r,t)}{\partial r}\bigg|_{r=R} = \frac{I}{F}, \quad \text{for } t \ge 0 \\ &D\frac{\partial C(r,t)}{\partial r}\bigg|_{r=R} = 0, \quad \text{for } t \ge 0 \end{aligned}. \tag{10}$$

2.2.1. Potentiostatic (constant voltage and surface concentration) operation

The analytic solution of the diffusion equation (Eq. (8)) with initial and boundary conditions for the potentiostatic control (Eq. (9)) is [32]:

$$\frac{C(r,t) - C_0}{C_R - C_0} = 1 + 2\sum_{n=1}^{\infty} \frac{(-1)^n}{n\pi x} \sin(n\pi x) e^{-n^2\pi^2\tau}, \tag{11}$$

where $x = r/R$ and $\tau = Dt/R^2$.

The average concentrations $C_{av}(r)$ and $C_{av}(R)$ are then given by

$$\frac{C_{av}(r) - C_0}{C_R - C_0} = 1 + \frac{6}{x^3}\sum_{n=1}^{\infty} \frac{(-1)^n}{n^3\pi^3} [\sin(n\pi x) - (n\pi x)\cos(n\pi x)] e^{-n^2\pi^2\tau}$$

$$\text{and} \quad \frac{C_{av}(R) - C_0}{C_R - C_0} = 1 - 6\sum_{n=1}^{\infty} \frac{1}{n^2\pi^2} e^{-n^2\pi^2\tau}. \tag{12}$$

Eq. (12) can be substituted into Eq. (3) to obtain the solutions for stresses under potentiostatic control:

$$\begin{aligned} \frac{\sigma_r}{[E\Omega(C_R - C_0)/(3(1-\nu))]} &= -4\sum_{n=1}^{\infty} e^{-n^2\pi^2\tau}\left(\frac{1}{(n\pi)^2} + (-1)^n\left(\frac{\sin(n\pi x) - n\pi x\cos(n\pi x)}{(n\pi x)^3}\right)\right) \equiv \zeta_r^V(x,\tau) \\ \frac{\sigma_\theta}{[E\Omega(C_R - C_0)/(3(1-\nu))]} &= -2\sum_{n=1}^{\infty} e^{-n^2\pi^2\tau}\left(\frac{2}{(n\pi)^2} + \frac{(-1)^n}{n\pi x}\sin(n\pi x) - (-1)^n\left(\frac{\sin(n\pi x) - n\pi x\cos(n\pi x)}{(n\pi x)^3}\right)\right) \equiv \zeta_\theta^V(x,\tau) \end{aligned} \tag{13}$$

where $\zeta_r^V(x,\tau)$ and $\zeta_\theta^V(x,\tau)$ are the respective dimensionless stresses in the radial and tangential directions for potentiostatic operation.

The mean and shear stresses are then given by

$$\frac{(\sigma_r + 2\sigma_\theta)/3}{[E\Omega(C_R - C_0)/(3(1-\nu))]} = -4\sum_{n=1}^{\infty} e^{-n^2\pi^2\tau}\left(\frac{1}{(n\pi)^2} + \frac{(-1)^n}{3n\pi x}\sin(n\pi x)\right) \tag{14}$$

and

$$\frac{\sigma_r - \sigma_\theta}{[2E\Omega(C_R - C_0)/(3(1-\nu))]} = \sum_{n=1}^{\infty} \frac{(-1)^n}{n\pi x} e^{-n^2\pi^2\tau}\left(\sin(n\pi x) - 3\left(\frac{\sin(n\pi x) - n\pi x\cos(n\pi x)}{(n\pi x)^2}\right)\right), \tag{15}$$

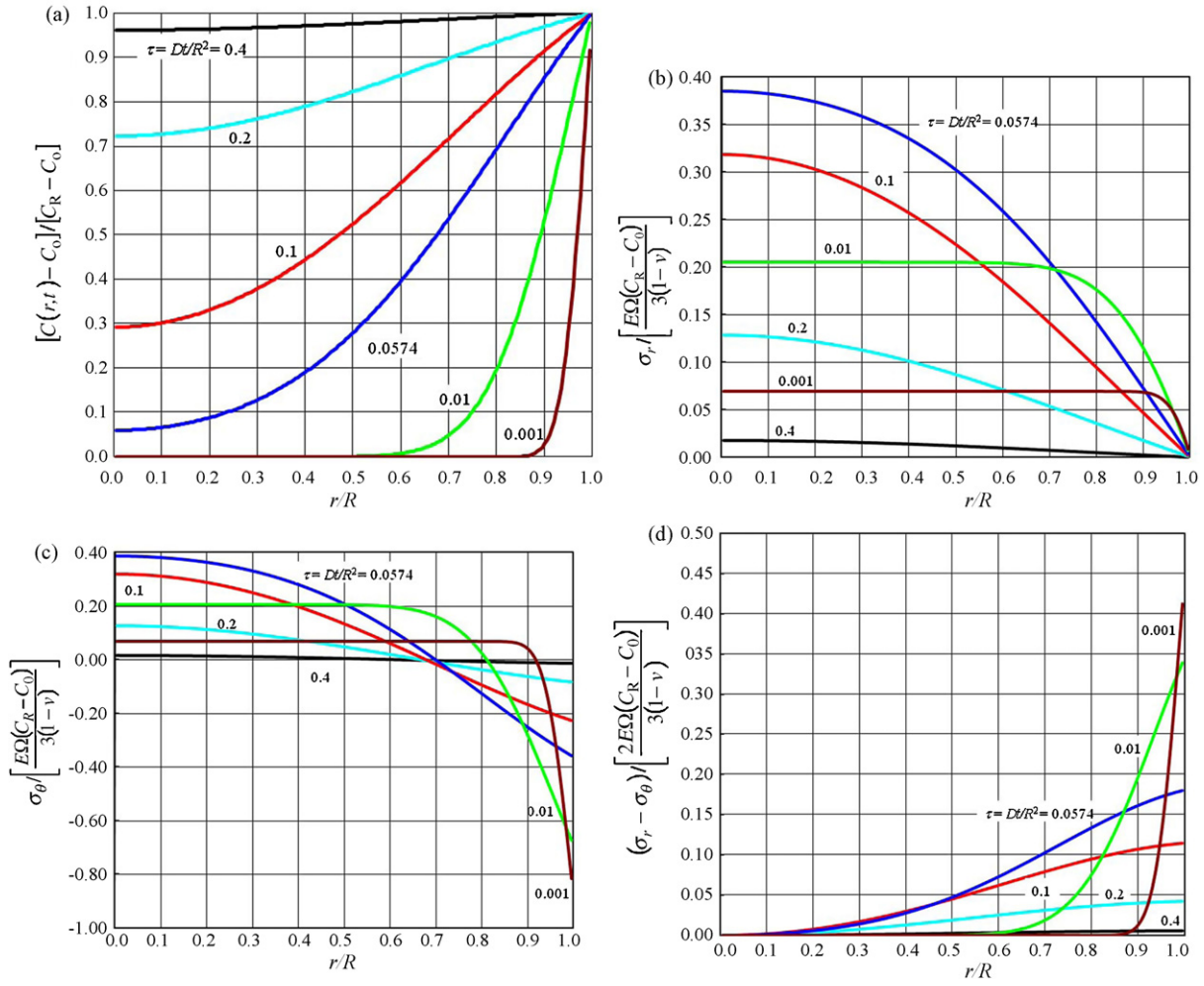

Fig. 1. Concentration profile (a) and the corresponding radial (b), tangential (c), and shear stress (d) for potentiostatic (constant solute surface concentration) control. The solution concentration increases with time (a), and the magnitudes of the tangential and shear stresses (c and d, respectively) at the particle surface decrease with time from 1 and 1/2, respectively, (cf. Eq. (3)) throughout the insertion process.

respectively. Fig. 1 shows the concentration, radial, tangential, and shear stresses, normalized by $E\Omega(C_R - C_0)/(3(1-\nu))$, as a function of position and time. Two cases of special interest are (1) "insertion" with initial condition $C_0 = 0$ and a finite C_R and (2) "extraction" with a finite C_0 and $C_R = 0$. For insertion, the radial stress is tensile in the sphere. At any given time, the tensile radial stress is the highest at the center and decreases monotonically to zero at the surface (Fig. 1b). It can be shown [25] that when the dimensionless time $\tau = Dt/R^2 = 0.0574$, which is just after the solute reaches the center of the sphere, the radial stress at the center attains the maximum:

$$\sigma_{r,\max} \approx 0.4\frac{E\Omega(C_R - C_0)}{3(1-\nu)}. \tag{16}$$

The radial stress at the center then deceases with increasing time. The tangential stress is compressive at the surface and tensile at the center of the sphere (Fig. 1c). The tensile tangential stress at the center appears before the solute reaches there. At the center, the tangential and radial stresses always have the same magnitude so that the stress at the center is purely hydrostatic in tension. The maximum tangential stress, which is compressive, occurs at the surface at time zero:

$$\sigma_{\theta,\max} = -\frac{E\Omega(C_R - C_0)}{3(1-\nu)}. \tag{17}$$

Analogous conclusions hold for extraction if "tensile" is replaced by "compressive". The shear stress at the center of the sphere is zero. For all times, the shear stress increases towards the surface. The maximum shear stress, with its magnitude half of that of the maximum tangential stress, occurs at surface at time zero (Fig. 1d):

$$\sigma_{shear,\max} = \frac{E\Omega(C_R - C_0)}{6(1-\nu)}. \tag{18}$$

Knowing the stresses, we can obtain the total elastic energy stored in the sphere E_T as a function of dimensionless time τ using Eqs. (6), (7) and (13):

$$\frac{E_T(\tau)}{2\pi R^3 E[\Omega(C_R - C_0)/(3(1-\nu))]^2} = \int_0^1 \left[\zeta_r^{V2}(x,\tau) + 2\zeta_\theta^{V2}(x,\tau) - 2\nu\zeta_\theta^V(x,\tau)(2\zeta_r^V(x,\tau) + \zeta_\theta^V(x,\tau))\right] x^2\,dx \equiv \Pi^V(\nu,\tau) \tag{19}$$

where $\prod^V$ is defined as the dimensionless total elastic energy in the sphere for potentiostatic operation. Eq. (19) is shown in Fig. 2 for representative values of Poisson's ratio ($-1 < \nu < 0.5$) for potentiostatically controlled charging. In a uniaxial tensile-strain test, the Poisson ratio ν is the ratio of lateral to longitudinal strain. It is dimensionless and typically ranges from 0.2 to 0.5. For incompressible materials, $\nu = 0.5$, and the material's volume remains constant under deformation. When stretching a material under uniaxial tension causes no lateral contraction, $\nu = 0$. For any stable material,

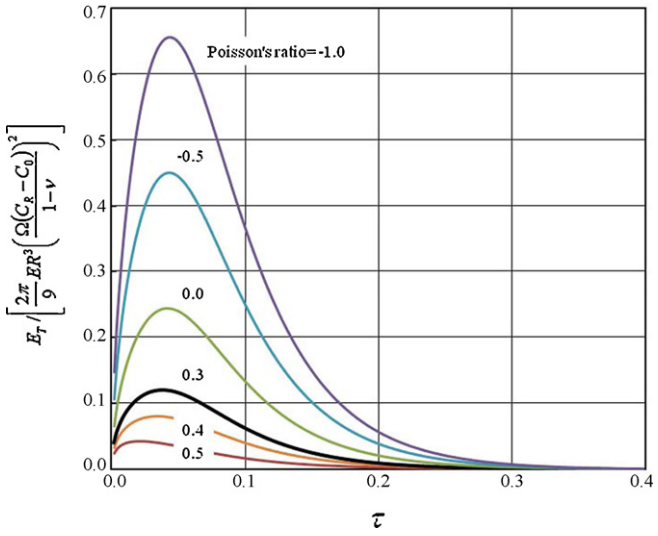

Fig. 2. Total strain energy vs. time for potentiostatic charging. The strain energy increases monotonically with decreasing Poisson ratios.

$-1 < \nu < 0.5$. Poisson's ratio affects the total stored energy significantly. The total strain energy first increases, reaches a maximum, and then decreases because of the transient nature of the stresses (Fig. 1b–d).

2.2.2. Galvanostatic (constant current and surface flux) operation

The analytic solution of the diffusion equation (Eq. (8)) with the initial and boundary conditions (Eq. (10)) for the galvanostatic condition is also well known [32][1]:

$$C(r,t) = C_0 + \frac{IR}{FD}\left[3\tau + \frac{1}{2}x^2 - \frac{3}{10} - \frac{2}{x}\sum_{n=1}^{\infty}\left(\frac{\sin(\lambda_n x)}{\lambda_n^2 \sin(\lambda_n)}\exp(-\lambda_n^2\tau)\right)\right], \tag{20}$$

where λ_n ($n = 1, 2, 3, \ldots$) are the positive roots of $\tan(\lambda_n) = \lambda_n$.

Using Eq. (20), we can express the average concentrations as

$$C_{av}(r,t) = C_0 + 3\left(\frac{IR}{FD}\right)\left[\tau + \frac{1}{10}(x^2-1) - \frac{2}{x^3}\sum_{n=1}^{\infty}\left(\frac{\sin(\lambda_n x) - (\lambda_n x)\cos(\lambda_n x)}{\lambda_n^4 \sin(\lambda_n)}\exp(-\lambda_n^2\tau)\right)\right],$$

$$C_{av}(R,t) = C_0 + 3\left(\frac{IR}{FD}\right)\tau = C_0 + 3\frac{I}{FR}t. \tag{21}$$

Eq. (21) can be substituted into Eq. (3) to obtain the solutions for stresses:

$$\frac{\sigma_r}{[(E\Omega/(3(1-\nu)))(IR/(FD))]} = \frac{1}{5}(1-x^2) + \frac{4}{x^3}\sum_{n=1}^{\infty}\left(\frac{\sin(\lambda_n x) - (\lambda_n x)\cos(\lambda_n x)}{\lambda_n^4 \sin(\lambda_n)}\exp(-\lambda_n^2\tau)\right) \equiv \zeta_r^I(x,\tau),$$

$$\frac{\sigma_\theta}{[(E\Omega/(3(1-\nu)))(IR/(FD))]} = \frac{1}{5}(1-2x^2) + 2\sum_{n=1}^{\infty}\frac{\exp(-\lambda_n^2\tau)}{\lambda_n \sin(\lambda_n)} \times \left(\frac{\sin(\lambda_n x)}{\lambda_n x} - \frac{\sin(\lambda_n x) - (\lambda_n x)\cos(\lambda_n x)}{\lambda_n^3 x^3}\right) \equiv \zeta_\theta^I(x,\tau). \tag{22}$$

where $\zeta_r^I(x,\tau)$ and $\zeta_\theta^I(x,\tau)$ are the respective dimensionless stress in the radial and tangential directions for galvanostatic operation.

The mean and shear stresses are then given by

$$\frac{(\sigma_r + 2\sigma_\theta)/3}{[(E\Omega/(3(1-\nu)))(IR/(FD))]} = \frac{1}{5}(1-2x^2) + \frac{4}{3x}\sum_{n=1}^{\infty}\left(\frac{\sin(\lambda_n x)}{\lambda_n^2 \sin(\lambda_n)}\exp(-\lambda_n^2\tau)\right) \tag{23}$$

and

$$\frac{\sigma_r - \sigma_\theta}{[(2E\Omega/(3(1-\nu)))(IR/(FD))]} = \frac{x^2}{10} + \frac{3}{x^3}\sum_{n=1}^{\infty}\left(\frac{\sin(\lambda_n x) - (\lambda_n x)\cos(\lambda_n x)}{\lambda_n^4 \sin(\lambda_n)}\exp(-\lambda_n^2\tau)\right) - \frac{1}{x}\sum_{n=1}^{\infty}\left(\frac{\sin(\lambda_n x)}{\lambda_n^2 \sin(\lambda_n)}\exp(-\lambda_n^2\tau)\right), \tag{24}$$

respectively.

Fig. 3 shows the concentration, radial, and tangential stresses, normalized by $E\Omega IR/(3(1-\nu)FD)$, as a function of position and time and using the sign convention defined in Eq. (10) for the current; i.e., insertion and extraction correspond to a positive and negative current, respectively. From a qualitative perspective, many of the observations described for the potentiostatic case (constant surface concentration) are seen for the galvanostatic (constant surface flux) case with some significant exceptions.

During insertion, the radial stress is tensile in the sphere. At any given time, the tensile radial stress is the highest at the center and decreases monotonically to zero at the surface. At any location, the tensile radial stress increases with time and tends to a "steady-state" (cf. Eq. (22)):

$$\sigma_{r,t\to\infty} = \frac{1}{5}(1-x^2)\left[\frac{E\Omega}{3(1-\nu)}\left(\frac{IR}{FD}\right)\right]. \tag{25}$$

The maximum tensile stress at the center of the sphere is $\sigma_{r,\max} = E\Omega IR/(15(1-\nu)FD)$. This is in contrast to the potentiostatic case where $\sigma_{r,\max}$ exhibits a transient behavior. The tangential stress is compressive at the surface and tensile at the center of the sphere. The tensile tangential stress at the center appears before the solute reaches there. At the center, the tangential and radial stresses always have the same magnitude so that the stress at the center is purely hydrostatic in tension. At any location, the tangential stress increases in magnitude with time and tends to a steady-state,

$$\sigma_{\theta,\max} = \frac{1}{5}(1-2x^2)\left[\frac{E\Omega}{3(1-\nu)}\left(\frac{IR}{FD}\right)\right]. \tag{26}$$

The maximum tangential stress is tensile at the center and compressive at the surface with the same magnitude as that of the maximum radial stress at the center, $|E\Omega IR/(15(1-\nu)FD)|$. The crossover from tensile to compressive tangential stress occurs at $x = 1/\sqrt{2}$ after the stress reaches the steady-state. Similar conclusions (i.e., replacing tension by compression) hold for extraction. The shear stress at the center of the sphere is zero. As was observed for the potentiostatic condition, the shear stress increases towards the surface

[1] The concentration $C(r,t)$ cannot exceed the concentration of available sites for the solute in the case of insertion electrodes, and this will place a limit on the admissible value of the product It.

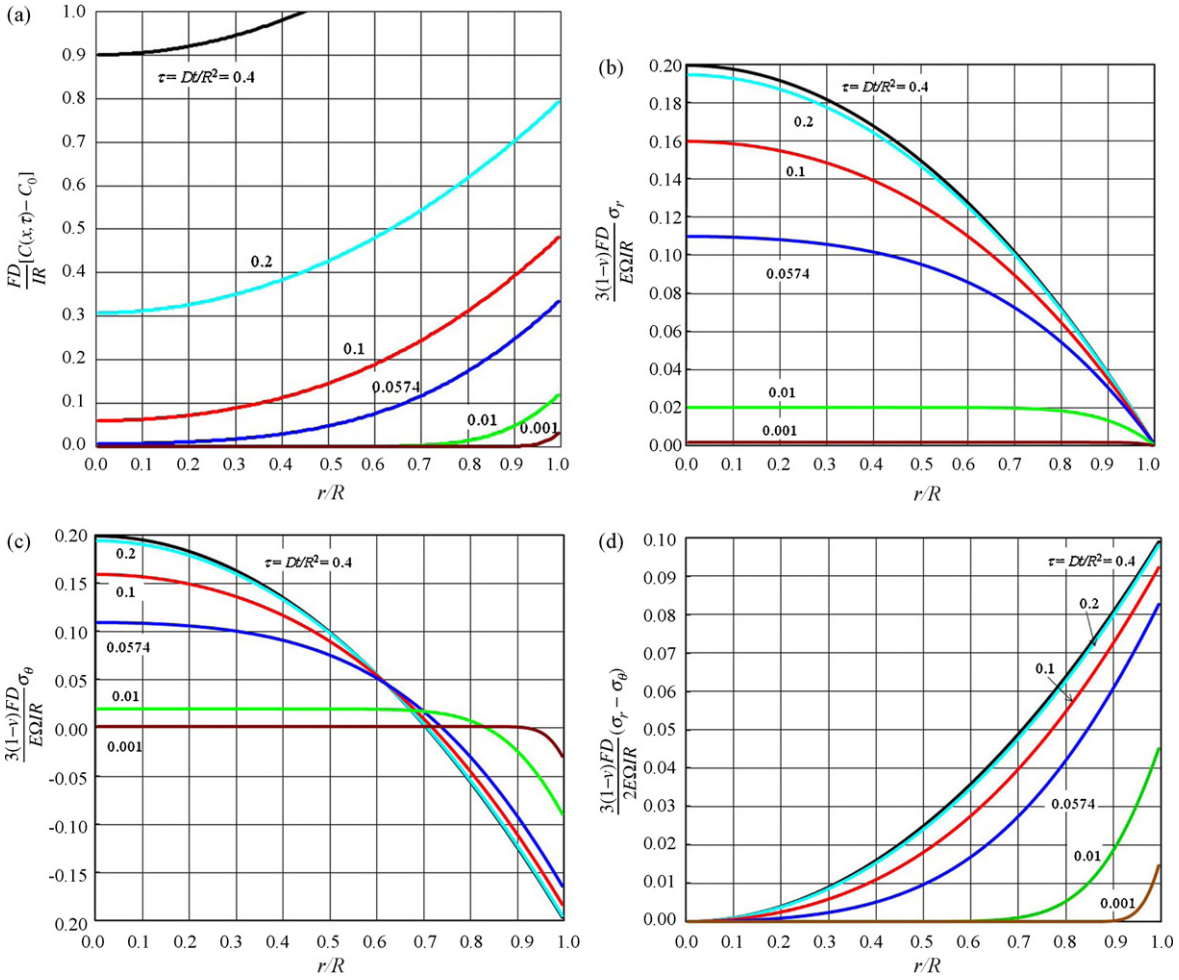

Fig. 3. Concentration profile (a) and the corresponding radial (b), tangential (c), and shear stress (d) for galvanostatic operation. The solution concentration increases with time (a), and the magnitudes of the tangential and shear stresses (c and d, respectively) at the particle surface increase with time throughout the insertion process. By comparing the analogous plots of Figs. 1 and 3, one can discern the very different character of the stress evolution for potentiostatic and galvanostatic control.

for all times. In addition, for all positions within the sphere, the shear stress increases with time. The maximum shear stress, with its magnitude half of that of the maximum tangential stress, occurs at surface after reaching the steady-state:

$$\sigma_{shear,\max} = \frac{1}{30}\left[\frac{E\Omega}{(1-\nu)}\left(\frac{IR}{FD}\right)\right] \tag{27}$$

The total dimensionless elastic energy stored in the sphere, Π^I, for galvanostatic operation can be expressed as

$$\frac{E_T(\tau)}{2\pi R^3 E[\Omega IR/(3(1-\nu)FD)]^2} = \int_0^1 \left[\zeta_r^{I2}(x,\tau) + 2\zeta_\theta^{I2}(x,\tau) - 2\nu\zeta_\theta^I(x,\tau)(2\zeta_r^I(x,\tau) + \zeta_\theta^I(x,\tau))\right] x^2\,dx \equiv \Pi^I(\nu,\tau) \tag{28}$$

Eq. (28) is shown in Fig. 4 for representative values of Poisson's ratio for galvanostatically controlled charging. Similar to the potentiostatic case, Poisson's ratio affects the total stored energy significantly. Unlike the potentiostatic case, however, the total strain energy increases monotonically to a steady-state consistent with the continuous increase in the stresses with time (Fig. 3b–d).

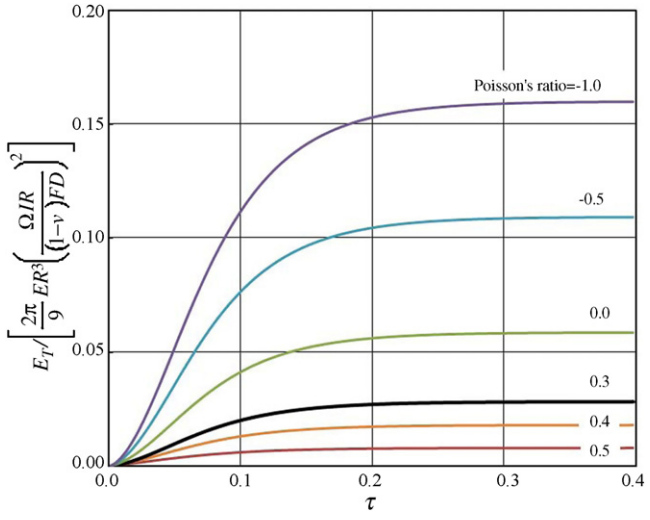

Fig. 4. Total strain energy vs. time for galvanostatic charging. While the strain energy increases monotonically with decreasing Poisson ratios, as is observed in the potentiostatic case (cf. Fig. 2), the evolution of the strain energy during galvanostatic control is quite different from that of potentiostatic control.

2.3. Implications for cell operation

There have been several recent studies optimized charging conditions [33–35]. Many of these studies focus on shortening the time to achieve a high state of charge (e.g., Ref. [33]). There is, however, little discussion on optimizing charging conditions to minimize mechanical stresses within the electrodes. The above analysis provides a guide to deciding between constant current and constant potential charging methods. Specifically, we can compare the maximum stresses encountered during either purely potentiostatic or galvanostatic conditions, subject to the assumptions used in the formulation the equations presented previously. The ratio of maximum radial stresses at the center is given by

$$\frac{\sigma_r^{\text{potentiostatic,max}}}{\sigma_r^{\text{galvanostatic,max}}} \approx 2\frac{C_R - C_0}{IR/(FD)} \tag{29}$$

Thus, the maximum radial stress under potentiostatic condition is greater than that under galvanostatic condition if the magnitude of current I is less than $2FD(C_R - C_0)/R$ and vice versa. Eq. (29) corresponds to the maximum radial stress shown in Fig. 1b (near $\tau = 0.0574$, cf. Eq. (17)) divided by the maximum radial stress of Fig. 3b (obtained from the steady-state solution, $E\Omega IR/(15(1-\nu)FD)$ per Eq. (25)). The constant 2 can be replaced by 1.93 if 3-digit accuracy is desired.

The ratios of maximum tangential stresses and shear stresses at the surface are the same and are given by

$$\frac{\sigma_\theta^{\text{potentiostatic}}}{\sigma_\theta^{\text{galvanostatic}}} = \frac{\sigma_{shear}^{\text{potentiostatic}}}{\sigma_{shear}^{\text{galvanostatic}}} = 5\frac{C_R - C_0}{IR/(FD)} \tag{30}$$

Thus, the maximum tangential or shear stress under potentiostatic condition is greater than that under galvanostatic condition if the magnitude of the current I is less than $5FD(C_R - C_0)/R$ and vice versa. Eq. (30) corresponds to the maximum tangential and shear stresses for a constant surface concentration (1 and 1/2, respectively, as can be seen by substituting C_0 for $C_{av}(R)$ and C_R for $C(R)$ in Eq. (3) for $t = 0$), respectively, divided by the maximum tangential and shear stresses of Fig. 3c and d, corresponding to $E\Omega IR/(15(1-\nu)FD)$ for the tangential stress and half this value for the shear stress, as described below Eq. (26).

In Fig. 5, we plot Eqs. (29) and (30) and show that $(C_R - C_0)FD/(IR)$ uniquely determines the maximum stress ratios for the radial, tangential, and shear stresses. The horizontal line at $\sigma^{\text{potentiostatic}}/\sigma^{\text{galvanostatic}} = 1$ delineates the parameter range of $(C_R - C_0)FD/(IR)$ such that $\sigma^{\text{potentiostatic}}/\sigma^{\text{galvanostatic}}$ is greater than or less than 1. Similarly, the ratio of maximum total strain energy can be obtained using Eqs. (19) and (28). Hence, the maxima in the curves depicted in Fig. 2 relative to those plotted of Fig. 4 (the long-time solution in the case of Fig. 4) yields the points depicted in Fig. 6 for $[(IR/FD)/(C_R - C_0)]^2(E_T^{\text{potentiostatic,max}}/E_T^{\text{galvanostatic,max}})$. This ratio of the maxima in total strain is seen to range from 4 to 5.5 for admissible values of the Poisson ratio.

These results show that $(C_R - C_0)FD/(IR)$ uniquely determines whether potentiostatic or galvanostatic charging would generate greater radial, tangential, and shear stress. It also determines which method generates greater total strain energy that can drive fracture in the spherical particle. This dimensionless parameter $(C_R - C_0)FD/(IR)$, representing the combined effects of materials properties (e.g., D), size (e.g., R), and charging conditions (e.g., C_R, C_0 and I), can therefore be used to guide the selection of charging conditions to minimize the maximum stresses and total strain energy experienced by an insertion electrode. We consider, for example, an electrode made of a brittle ceramic material that fractures due to tensile stresses. Eq. (29) can then be used to select a charging condition, either purely potentiostatic or galvanostatic, which gives rise to a lower tensile stress. In contrast, since plastic deformation is usually the dominant failure mechanism for metallic alloy electrodes, Eq. (30) can be used to select a charging condition resulting in a lower shear stress. Thus, depending on the failure mode of the electrode material, e.g., tensile fracture or shear induced plastic deformation, an appropriate charging method may be selected, and the best regime may consist of a combination of potentiostatic and galvanostatic conditions.

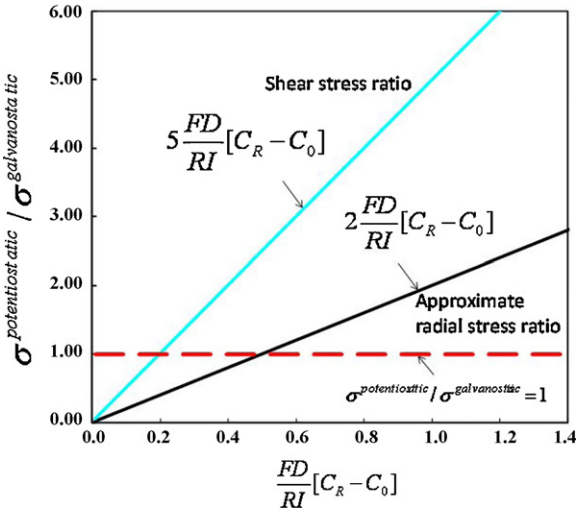

Fig. 5. A map showing the ratio of maximum stresses under potentiostatic and galvanostatic control vs. a dimensionless parameter, $(C_R - C_0)FD/(IR)$, which represents the combined effects of materials properties (e.g., D), size (e.g., R), and charging conditions (e.g., C_R, C_0, and I). Hence this map allows one to comprehend how changes material or process parameters can be employed to stay below specified stress values. The constant 2 appearing in the label for the radial stress ratio can be replaced by 1.93 if 3-digit accuracy is desired.

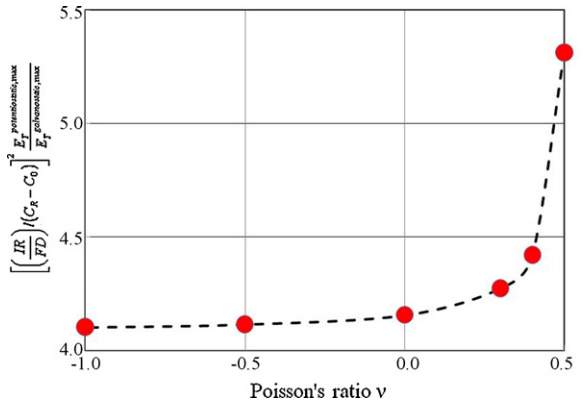

Fig. 6. Ratio of maximum total strain energy as determined by Eqs. (19) and (28). The dashed line is provided as a guide and does not represent calculations.

3. Summary

We have developed analytic expressions for stress evolution in a spherically shaped electrode element under either galvanostatic or potentiostatic conditions. We show that stresses evolve quite differently for the two conditions when solute diffusion resistance dominates within host particles.

- For potentiostatic control, the magnitude of radial and tangential stresses at any location increases initially and then decreases with time. The total strain energy, which drives particle fracture, experiences a similar trend.

- For galvanostatic control, the magnitude of radial and tangential stresses at any location increases and then reaches a steady-state value that is independent of time. The total strain energy also increases monotonically to a finite value.

The maximum stresses and total strain energy attained under potentiostatic and galvanostatic conditions are compared and contrasted. This analysis suggests a possibility of developing new battery charging strategies that minimize stresses and thus prolong battery life.

Acknowledgements

We would like to thank Stephen Harris and Adam Timmons for helpful discussions.

References

[1] S. Prussin, J. Appl. Phys. 32 (1961) 1876.
[2] J.C.M. Li, Metall. Trans. A9 (1978) 1353.
[3] S.B. Lee, W.L. Wang, J.R. Chen, Mater. Chem. Phys. 64 (2000) 123.
[4] W.L. Wang, S. Lee, J.R. Chen, J. Appl. Phys. 91 (2002) 9584.
[5] S.-C. Ko, S. Lee, Y.T. Chou, Mater. Sci. Eng. A409 (2005) 145.
[6] F.Q. Yang, J.C.M. Li, J. Appl. Phys. 11 (2003) 9304.
[7] F.Q. Yang, Mater. Sci. Eng. A409 (2005) 153.
[8] M. Doyle, T. Fuller, J. Newman, J. Electrochem. Soc. 140 (1993) 1526.
[9] T. Fuller, M. Doyle, J. Newman, J. Electrochem. Soc. 141 (1994) 1.
[10] M. Doyle, J. Newman, J. Electrochem. Soc. 143 (1996) 1890.
[11] R. Darling, J. Newman, J. Electrochem. Soc. 144 (1997) 4201.
[12] D.R. Baker, M.W. Verbrugge, J. Electrochem. Soc. 146 (1999) 2413.
[13] V. Srinivasan, J. Newman, J. Electrochem. Soc. 151 (2004) A1530.
[14] S. Devan, V.R. Subramanian, R.E. White, J. Electrochem. Soc. 151 (2004) A905.
[15] D. Dees, E. Gunen, D. Abraham, A. Jansen, J. Prakashb, J. Electrochem. Soc. 155 (2008) A603.
[16] R.E. García, Y.-M. Chiang, W.C. Carter, P. Limthongkul, C.M. Bishop, J. Electrochem. Soc. 152 (2005) A255.
[17] J. Christensen, J. Newman, J. Electrochem. Soc. 153 (2006) A1019.
[18] J. Christensen, J. Newman, J. Solid State Electrochem. 10 (2006) 293.
[19] X. Zhang, W. Shyy, A.M. Sastry, J. Electrochem. Soc. 154 (2007) A910.
[20] X. Zhang, A.M. Sastry, W. Shyy, J. Electrochem. Soc. 155 (2008) A542.
[21] D. Zhang, B.N. Popov, R.E. White, J. Electrochem. Soc. 147 (2000) 831.
[22] Y.-T. Cheng, M.W. Verbrugge, J. Appl. Phys. 104 (2008) 083521.
[23] M.W. Verbrugge, Y.-T. Cheng, Electrochem. Soc. (ECS) Trans. 16 (2008) 127.
[24] "Basic Research Needs for Electrical Energy Storage - Report of the Basic Energy Sciences Workshop for Electrical Energy Storage" chaired by John B. Goodenough (Office of Basic Energy Sciences, Department of Energy, July 2007). This report is available on the web at http://www.sc.doe.gov/bes/reports/files/EES_rpt.pdf.
[25] S.P. Timoshenko, J.N. Goodier, Theory of Elasticity, 3rd edition, McGraw-Hill, New York, 1970.
[26] M.W. Verbrugge, B.J. Koch, J. Electrochem. Soc. 150 (2003) A374.
[27] A.J. Bard, L.R. Faulkner, Electrochemical Methods, Wiley, New York, 1980.
[28] J. Newman, K.E. Thomas-Alyea, Electrochemical Systems, 3rd edition, Wiley, 2004.
[29] M.W. Verbrugge, B.J. Koch, J. Electrochem. Soc. 143 (1996) 24.
[30] M.W. Verbrugge, B.J. Koch, J. Electrochem. Soc. 143 (1996) 600.
[31] M.W. Verbrugge, B.J. Koch, J. Electrochem. Soc. 146 (1999) 833.
[32] H.S. Carslaw, J.C. Jaeger, Conduction of Heat in Solids, 2nd edition, Clarendon Press, Oxford, 1959.
[33] B.K. Purushothaman, U. Landau, J. Electrochem. Soc. 153 (2006) A533.
[34] N.K. Poon, B.M.H. Pong, C.K. Tse, IEEE Trans. Power Electron. 18 (2003) 1262.
[35] L.R. Chen, J.J. Chen, N.Y. Chu, G.Y. Han, IEEE Trans. Power Electron. 55 (2008) 2482.